Available online www.jocpr.com

Journal of Chemical and Pharmaceutical Research, 2019, 12(2):14-32

Research Article

ISSN: 0975-7384
CODEN(USA): JCPRC5

Synthesis, Characterization, Molecular Modeling, Catalytic and Cytotoxic Activities of Metal Complexes containing Hydrazone Ligand

Mohamed I Ayad[1], Abdel-monsef IA[1*], Marwa H Gendia[1] and Abd-Allah Sh El-Etrawy[2]

[1]Chemistry Department, Faculty of Science, Menoufia University, Egypt

[2] Department of Organic Chemistry, Basic Science Center & College of Pharmacy & Drug manufacturing, Misr University for Science &Technology (MUST), Egypt

---

ABSTRACT

Novel Schiff base ligand of type [H_2L] was prepared by the condensation of acetoacetanilide with nicotinic hydrazide. The metal complexes of Co^{+2}, Ni^{+2}, Cu^{+2}, $Mn^{+2}$and Zn^{+2} were characterized and investigated by physical and spectral techniques, namely, elemental analysis, melting point, conductivity, ^1H NMR, IR, UV-Vis spectra, ESR, as well as x-ray diffraction, TEM and photo catalytic activity under UV visible irradiation were performed. They were further analyzed by thermal technique (TGA/DTA) to gain better insight about the thermal stability and kinetic properties of the complexes. Thermal data revealed high thermal stability and nonspontaneous nature of the decomposition steps. The molar conductance values were relatively low, showing their non-electrolytic nature. To study the cytotoxicity of the ligand and some of its metal complexes against human liver cancer cell (HePG-2 cell line). The cells were dosed with the complexes at varying concentrations and cell viability was measured by sulfo-rhodamine-B stain (SRB) method. The compounds show marked antiproliferative effect compared with a standard drug (vinblastine).

Keywords: Acetoacetanilide; Nicotinic hydrazide; Schiff base; Complexes; Catalytic; Cytotoxic activity

---

INTRODUCTION

Hydrazones and their metal complexes was widely studied due to their versatile applications in the field of analytical and medicinal chemistry [1,2]. Hydrazone ligands can act as bidentate, tridentate or tetradentate ligands depending on the nature of heterocyclic ring substituents attached to the hydrazone unit.

These ligands due to their facile keto-enol tautomerization and the availability of several potential donor sites can coordinate with metals. Hydrazides and hydrazones have interesting ligation properties due to presence of several coordination sites [3]. Coordination chemistry of metal complexes of hydrazones [4], has gained a special attraction due to their biological activity and their ability to act as potential inhibitors for many enzymes [5,6]. The presence of heterocyclic rings in the synthesized hydrazones plays a major role in deciding the extent of their pharmacological properties [7].

Hydrazone ligands create environment similar to biological systems by usually making coordination through oxygen and nitrogen atoms. These ligands can coordinate with metal ions to produce stable metal complexes owing to their facile keto-enol tautomer. Their metal complexes have also been proposed as acid base indicators, reservoir sensors [8] and as analytical reagents [9] because of the color intensification, which accompanies deprotonation.

In this paper we describe the synthesis, characterization, catalytic and cytotoxic activities studies of some divalent metal ion complexes based on Schiff base derived from condensing nicotinic acid hydrazide with acetoacetanilide (H_2L).

MATERIALS AND METHODS

Materials and Physical Measurements

All chemicals and solvents used were pure chemicals from BDH or Aldrich and used as received. Elemental analyses (C, H, N and Cl) were carried out at the Micro analytical Unit of the Cairo University. Metal ions were determined using atomic absorption with a Perkin Elmer (model 2380) spectrophotometer. The IR spectra were measured as KBr discs using a Perkin-Elmer 1430 infrared spectrometer (4000-400 cm^{-1}). Electronic absorption spectra in the 200-900 nm regions were recorded on a Perkin-Elmer 550 spectrophotometer. The thermal analyses (DTG and TGA) were carried out on a Shimadzu DT-30 and TG-50 thermal analyzers in the 27-800ºC range at a heating rate of 10ºC min^{-1}. The magnetic susceptibilities were measured at room temperature using the Gouy method with mercuric tetra thiocyanatocobaltate (II) as magnetic susceptibility standard; diamagnetic corrections were made using Pascal's constants. ESR measurements at room temperature were carried out using Joel spectrometer model JES-FE 2XG equipped with an E101 microwave bridge. DPPH was used as a standard material. A Bibby conductimeter MCl was used for conductance measurements. The TEM images of complexes were taken in a transmission electron microscope (JEOL model 1200 EX) at Central Laboratory, Faculty of Science, Menoufia university, Shebin El-kom, Egypt. The X-ray powder diffraction patterns were recorded using a Philps pw-1729 (Cu k_a radiation (λ) 1.54178 A˚ using Ni filter) and Deby-Scherrer pw 1050.

Synthesis of the Ligand and Its Complexes

The acetoacetanilidene nicotinyl hydrazone ligand (H_2L) was prepared by mixing ethanolic solutions of acetoacetanilide (0.05 mol) and nicotinic acid hydrazide (0.1 mol) with reflux for 3 hrs. The resulting product was filtered off and crystallized from ethanol (yield 85%).

The complexes were prepared by the following general method. To a hot ethanolic solution of Acetoacetanilidene nicotinyl hydrazone 0.05 ml of metal salts ($MCl_2 \cdot nH_2O$) were added where M=Mn(II), Co(II), Ni(II), Cu(II) and Zn(II) in 1M:1L and 2M:1L stoichiometric ratio. The reaction mixture was refluxed on a water bath for 5 hours. The formed complexes were filtered off, washed several times with pure dry methanol and dried under vacuum over anhydrous $CaCl_2$.

Catalytic Study

The catalytic study of the metal complexes were recorded as previously reported [10,11].

Cytotoxic Activity

The Antiproliferative activity of the ligand and some of its metal complexes was evaluated *in vitro* against cell lines of Hep-G2 (human liver cancer) using the SulfoRhodamine-B-stain (SRB) assay published method in the Pathology Laboratory, Pathology Department, Faculty of Medicine, El-Menoufia University, Egypt. Cells were plated in the 96-multiwell plate (104 cells/ well) for 24 h. before treatment with the compounds to allow attachment of cell to the wall of the plate. Different concentrations of the compounds under test in DMSO (0, 5, 12.5, 25 and 50 µg ml^{-1}) were added to the cell monolayer, triplicate wells being prepared for each individual dose. Monolayer cells were incubated with the complexes for 48 h at 37°C and under 5% CO_2. After 48 h. cells were fixed, washed and stained with SRB-stain. Excess stain was washed with acetic acid and attached stain was recovered with Tris-ethylenediamine-tetraacetic acid buffer. Color intensity was measured in an enzyme-linked immunosorbent assay reader. The relation between surviving fraction and drug concentration is plotted to get the survival curve for each tumor cell line after addition the specified compound.

RESULTS AND DISCUSSION

Characterization of the Ligand and Its Complexes

The acetoacetanilidene binicotinyl hydrazine ligand (H_2L), was obtained as a pure solid compound. The analytical and physical data were shown in Table 1. The prepared ligand is air stable and partially soluble in most common organic solvent as MeOH, EtOH. CH_3OH, benzene and CCl_4 and soluble in DMF and DMSO. The data reveals that the ligand (H_2L) may in principles exhibit keto-enol tautomerism involving the two –CO–NH– groups giving the following tautomerism (Figure 1).

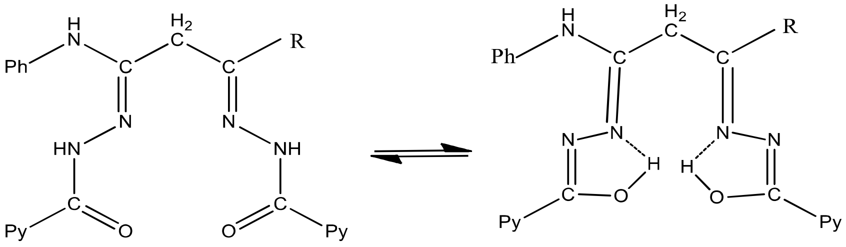

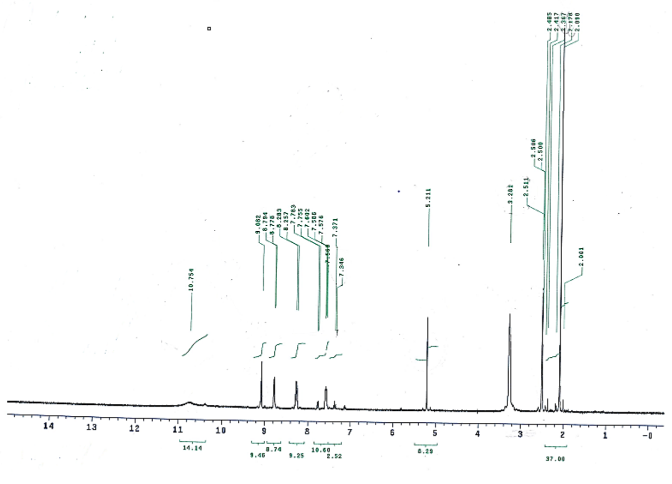

Figure 1. The ^{1}H-NMR spectrum of free organic ligand in $CDCl_3$ at room temperature, the spectrum displays signals at

δ=1.76, 1.94 (CH_2 and CH_3), 6.3-7.2 (aromatic protons), 7(2 NH) and at 8.2-9.1 (Nicotinyl group)

The divalent Cu and Ni complexes are prepared as (1M:1L) one metal to one ligand and the divalent Mn complex was obtained as (2M:1L) two metal to one ligand molecule. Whereas, Co and Zn complexes were obtained in two forms (1M:1L) and (2M:1L) in which the ligand acts as dibasic tetra dentate towards the divalent metal ions. All the complexes are insoluble in most common organic solvents and soluble in DMF and DMSO. The water contents reflect the existence of lattice and coordinate water molecule for the prepared complexes. The calculated and the found values of elemental analysis are in satisfactory agreement with each other with high accuracy supporting the suggested molecular formulae in Table 1.

Table 1. Elemental analysis of ligand and its complexes

	Compounds	Color m.wt	m.p°c	Elemental analysis(found) calcd				A_m ohm^{-1} cm2mol^{-1}
				C %	H%	N%	M%	
	H_2L 0.5 EtOH.0.5H_2O	Beige 447	160	[61.7] 62.63	[5.6] 6.66	[21.9] 22.27		
1	$[Cu(H_2L)(Cl_2)]$ 3.5H_2O	Dark green 612.5	>250	[43.13] 43.24	[4.90] 4.53	[16.00] 13.04	[10.52] 10.36	41
2	$[Ni(H_2L)(Cl_2)]$ 4H_2O	light green 617.12	>250	[42.70] 40.65	[4.70] 4.78	[15.88] 15.83	[9.4] 9.84	25.5
3	[Co(L)] 2.5H_2O.0.5EtOH	Dark green 540	>250	[51.10] 51.04	[5.00] 5.78	[18.15] 18.15	[11.16] 10.9	20.17
4	[Zn (L)] 3.5H_2O	Beige 541.84	>250	[48.72] 48.59	[4.80] 4.99	[18.10] 19.05	[12.15] 12.07	40.26
5	$[Mn_2(H_2L)(Cl_4)(H_2O)_2]$ H_2O	Beige 719.41	>250	[36.6] 37.15	[3.7] 3.7	[13.60] 13.68	[14.54] 15.25	63.2
6	$[Co_2(H_2L)(Cl_4)(H_2O)_2]$	Dark green 709.59	>250	[37.20] 37.51	[3.52] 2.92	[13.81] 14.27	[16.52] 16.33	17.6
7	$[Zn_2(L)(Cl_2)]$ 3H_2O	Beige 670	>250	[39.4] 38.96	[4.00] 3.99	[14.6] 14.33	[19.9] 20.3	43.4

IR Spectra

The IR data of ligand (H_2L) are listed in Table 2. It depicts prominent bands exhibits frequencies of υ OH and out of plane δ OH at 3398 and 977 cm^{-1}. The broad high intensity band of υ OH appears at lower frequency than expected denoting the contribution of OH group in hydrogen bonding. Whereas, the two medium bands at 3209 and 3016 cm^{-1} were assigned to υ (NH) group [12]. Two shoulder and strong band occurring at 1671 and 1648 cm^{-1} are assigned to υ (C=O) group. These observations confirmed the ketonic form of the ligand in the solid state [13]. The band at 1603 cm^{-1} is due to υ (C=N) of the azomethine group [14]. The bands observed at 1542-1477 cm^{-1} are assigned υ (C=O) of amide C=ONH and δ NH. In addition, the bands observed at 1327, 1307, 1033 and 709 cm^{-1} may attributed to υ (C-O), γ C-O ring vibration and γ NH-C=O respectively. The absence of OH stretching and bending vibration of frequency of acetoacetanilide moiety of the AANH appearing in the range 3600-3220 cm^{-1} and 1330 cm^{-1} respectively, indicate that the enolic carbonyl group is not involved in the reaction and only the imide carbonyl group participate in the condensation. By comparison of the IR spectra of complexes with that of the free ligand, It was concluded that, all complexes and ligand showed broad bands around (3460-3398 cm^{-1}) indicating the presence of lattice water (hydrated, coordinated). The bands due to υ (N-H) at 3209-3016 cm^{-1}, amide II increase in frequency (1542-1520) and amide III splits into components at 1272-1198 cm^{-1} and 1406-1318 cm^{-1}. These changes in amide group vibrations suggest amide oxygen coordination to metal ion as well as coordination of ligand in keto form except complexes 3,4 [15-18]. The two bands due to υ NH and υ (C=O) stretches showed that a small shift is observed for the υ (C=O) and υ NH bands which implies that the ligand is coordinated in the keto form for the remaining complexes. The υ (C=N) bands of the complexes are found in the range 1607-1612 cm^{-1} are shifted to small frequency by 3-9 cm^{-1}, indicating the coordination of azomethine nitrogen to the metal [19]. The increase in υ (N-N) bands in complexes due to the increase in double bond character confirm the coordination of the ligand through the azomethine nitrogen [20]. The IR spectra of complexes (3,4) exhibits new band appearing in the region 1406-1332 cm^{-1} and 1525-1488 cm^{-1} assigned to υ (C-O) and υ (N=C-O) indicating the involvement of the original carbonyl oxygen in bonding as an enolate form [21] with loss of enolic proton up on complexation. On the other hand, the characteristic υ (N-N) band was found to be shifted from 1033 cm^{-1} in the spectrum of the ligand to 1051 cm^{-1} in the spectra of complex 3,4. This shift may be ascribed to the fact that the electron attracting ketonic group is absent in these complexes the situation led to an increase in the electronic density on the nitrogen atom. In the spectra of complexes 5-7 the presence of a band at 778-771 cm^{-1} is assigned to Zn-Cl-Zn [22].

Table 2. IR frequencies of the bands of the ligand and its metal complexes

No.	N (H_2O)	N (NH)	υ (CO) Amide I	ν (C=N)	ν (C=N)	δ NH amide	ν (N-N)	ν (M- N)	ν (M-O)
H_2L	3398	3209(m) 3016	1648 (s)	1603 (sh)	-	1476	1033	-	-
(1)	3449 3347	3082 (m) 2930	1683 (s)	1611(sh)	1539 (m)	1486	1061	465 (w)	511 (w)
(2)	3500 3314 (b)	3076 (m) 2977	1661 (s)	1601(sh)	1527 (m)	1482 1396	1045	451 (w)	510 (w)
(3)	3500 3350(b)	2930 (m)	1652 (s)	1612 (sh)	1520 (m)	1473 1402	1047	430 (w)	512 (w)
(4)	3314	3212	1663	1526		1475	1055	434	517
(5)	3500 3403(b)	3240 (m) 3024	1651 (s)	1612 (Sh)	1554 (w)	1485 1318	1045	426 (w)	502 (w)
(6)	3394	3212	1660	1536		1480	1044	430	544
(7)	3441(b)	3112 2933	1651 (m)	1616 (m)	1525 (Sh)	1475 1406	1051	424 (w)	504 (w)

Electronic absorption spectra and magnetic moments

The spectrum of the ligand in DMF shows intense bands at 296 and 320 nm assigned to the π-π^* transition of benzene, pyridine ring, and azomethine group respectively [23,24], while the band appearing at the range 392-431 nm may be assigned to the n-π^* transition. All the complexes show strong absorption bands at 320-336 nm and 354-402 nm which can be associated with intra-ligand charge transfer transition C.T. [23]. The electronic spectrum of copper (II) complex shows broad bands at 444-532 and 610-650 nm which are assigned to ligand metal charge transfer ${}^2B_1$-${}^2E_g$, ${}^2B_1$-${}^2B_2$ transitions respectively, indicating a distorted octahedral structure [25,26]. The observed magnetic moment value of Cu (II) complex is 1.88 B.M. which confirms the above geometry. The electronic spectrum of nickel (II) complex shows two distinct bands which are assignable to the spectral features of octahedral Ni (II) complex. The broad bands in the range 697-767 nm and 600 nm are assigned to octahedral symmetry [27] corresponding to ${}^3A_{2g}(f)\rightarrow{}^3T_{1g}(f)$ and ${}^3A_{2g}(f)\rightarrow{}^3T_{1g}(p)$ transition. The Ni (II) complex has magnetic moment value of 3.1 B.M. which confirms the above geometry. The magnetic moment value of Co (II) complex is 4.26. The value reported is consistent with octahedral arrangement. The spectrum in DMF solution exhibits a band sit 545 nm, 600 nm and 617 nm indicating distorted octahedral geometry transition and a weak band at 668 nm due to spin-orbit coupling [28]. The electronic spectra of Mn (II) complex in DMF solution displays bands 402 nm, 408 nm and 480 nm 512 nm and 590 nm corresponding to $^6A_{1g}$(f) →T_{2g} (^{4}G), $^6A_{1g}$ (f) → $^4A_{1g}$,^4E_g(^{4}G), $^6A_{1g}$ (f) → $^4T_{1g}$(^{4}G). These bands assigned to octahedral coordinate geometry around Mn (II) [29,30]. The lower magnetic moment value 1.85 BM may be due to low spin state together with metal–metal interacting [31,32]. The Zn (II) complex shows bands at 336 nm and 431 nm due to ligand-metal charge transfer and the tetrahedral structure was proposed Table 3.

Table 3. Electronic absorption spectral data and magnetic moments of the ligand and its metal complexes

	λ_{max} (nm)	**μ_{eff} (B.M)**
H_2**L**	296, 320 and 392	
1	296, 314, 385, 398, 410, 570, 760	1.76
2	296, 317, 337, 344, 374, 450, 700	4.2
3	294, 299, 392, 471, 508, 583, 648, 683	
4	312, 420, 487, 918	
5	296, 335, 344, 374, 402, 408, 430, 480, 512, 590	1.85
6	296, 340, 386, 510, 545, 600, 617, 668	3.77
7	296, 325, 336, 374, 431, 460	

ESR of the Cu (II) Complex (1)

ESR spectrum of Cu (II) complex is shown in Figure 2 was performed at room temperature to obtain further information about the stereochemistry and the nature of the metal. Ligand bonding in addition to determine the spin-spin interaction between Cu (II) complex is characteristic of an axial symmetry with two (g) values ($g_{\|}$=2.21, $g_{\perp}$=2.033) and the observed trend is $g_{\|}>g_{\perp}>g_e$=2.0023, This corresponds to tetragonal distorted octahedron structure with (d_{x2-y2}) giving $^2B_{1g}$ as aground state [33]. The lower value of ($g_{\|}$) than 2.30 is indicative of covalent character of bonding between copper (II) ion and the ligand. Also, the exchange interaction between copper (II) ions can be calculated for axial symmetry using the expression ($G= g_{\|}-2.0023/g_{\perp}-2.0023=4$).

The (G) value for this complex is greater than four (6.35) clarifies the absence of exchange coupling between Cu (II) ions [34]. This is compatible with its magnetic moment value Table 3. The spectrum of Cu (II) complex depicts hyperfine anisotropy signal with well-defined hyperfine splitting on the low field region with (A‖=154.8 × 10-4 cm^{-1}) this is may be due to interaction between the spin of unpaired electron (s=1/2) of Cu(‖) ion and its nuclear spin (I=3/2). Also, the ESR spectrum exhibits weak hyperfine splitting on the high field region with ($A_{\perp}$= 28.51 × 10^{-4} cm^{-1}). The empirical factor ($f=g_{\|}/A_{\|}$) can be calculated to determine the tetragonal distortion degree. The (f) value was found (142.76 cm) implying to distorted octahedron structure of Cu (II) ion [35].

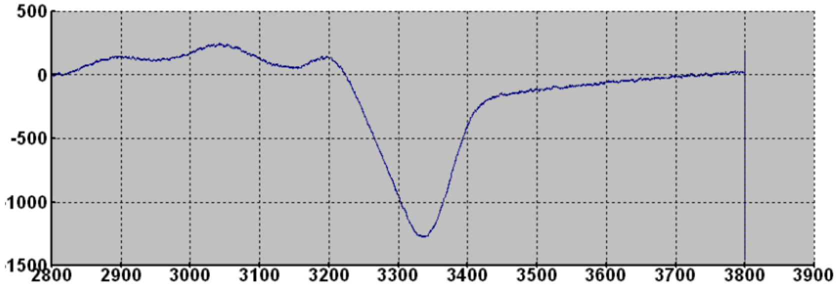

Figure 2. ESR spectrum of Cu (II) complex

Thermal Analysis

In order to characterize metal complexes more fully in terms of thermal stability. Their thermal behavior were carried out to study thermal decomposition of the solid compounds and support their molecular structures and to identify the different types of solvents of crystallization TGA and DTG curves of investigated complexes are given in Figure 3 and the data of thermal analysis are also collected in Table 4.

From TGA and DTG curves of the hydrated ligand $H_2L.0.5H_2O.0.5EtOH$ showed thermal stability up to 49°C, Then the pattern exhibits an estimated weight loss of 7.14% within temperature range 49-172°C, with DTG peak at (T_{max}=84°C) assigned to removal of 0.5 mole ethanol and 0.5 mole of water of crystallization. The ligand pyrolysis starts at range 172-265°C attributed to partial decomposition of ligand (47.4% calcd., 47.46% found) which may be due to mass loss of the corresponding to ($C_{12}H_8N_2O_2$). A broad endothermic peak in DTG was observed for this step the remaining part from the ligand pyrolysis, indicating weight loss of (42.28% calcd., 42.42% found) due to organic residue ($C_9H_{11}N_5$) at range (265-562°C).

The complex 1 and 2 showed weight loss of (10.2% calcd., 15.4% found) which corresponding to three and half water molecules for complex 1 in the temperature range (27-217°C), and four water molecules for complex 2 in the temperature range (30-290°C) indicate the presence of lattice water in these complexes. The second step occurs within the temperature range (217-285°C) for complex 1 and (290-412°C) for complex 2 with the estimated mass losses 11.55% for 1, 10.78% for 2 (calculated mass losses 11.59%, found 11.00%) may be attributed to the loss of Cl_2. This is confirmed by the experiment TGA weight loss and DTG curve which gave an endothermic (broad/weak) peaks. Afterward a progressive decrease in TGA mass losses from (643-756°C) for complex 1(674-900°C), for complex 2 assigned to complete decomposition with formation of metal oxides (i.e., CuO and NiO) respectively [36,37].

Complexes 3,4 showed a weight loss of 12.62% for complex 3 and 11.64% for complex 4 in the temperature range 31-225°C assigned to loss of 2.5 moles of water and 0.5 EtOH for complex 3, 3.5 moles of water for complex 4.

Then, the partial ligand pyrolysis takes place up to 530°C and complete ligand pyrolysis of the complex forming CoO and ZnO. In addition, the thermal properties of binuclear metal complexes were investigated by TGA and DTG presents the recorded TGA/DTG curves of metal (II) complexes in nitrogen atmosphere and important data are summarized in Table 4.

Complex 5 shows two successive weak endothermic peak from 33-77.5°C with a weight loss of 2.5% which is due to the loss of one molecule of hydrated water, The second peak from 77.5-118°C with a weight loss of 5% which is due to the loss of two coordinated water molecules. The anhydrous complex loss the two chloride molecules at temperature range 118-305°C with weight loss 9.7%. The third step with the temperature range 305-364°C with the estimated mass lose 38.7% corresponding to two chloride molecules and partial pyrolysis of ligand. Finally at the temperature range from 364-700°C, the broad band with weight loss 19.69% calcd, 18.3% found corresponding to complete pyrolysis of the ligand moiety and formation of 2MnO as a final product.

Complex 6 exhibits a weight loss at temperature about 31-130°C as indicated from TGA and DTG curves which display a weight loss (5.06% calcd., 5.07% found) corresponding to removal of the two water molecules. The second step of decomposition starts at 130°C and extended up to 387°C corresponding to the loss of four Cl atoms (19.98% calcd. 20.00% found). While, the third one starts from 387°C up to 567°C due to complete degradation of organic matter ($C_{22}H_{21}N_7$) with percentage weight loss (53.60% calcd. 53.46 % found) and ended with the formation of (2CoO) as a final product (21.08% calcd. 21.05% found).

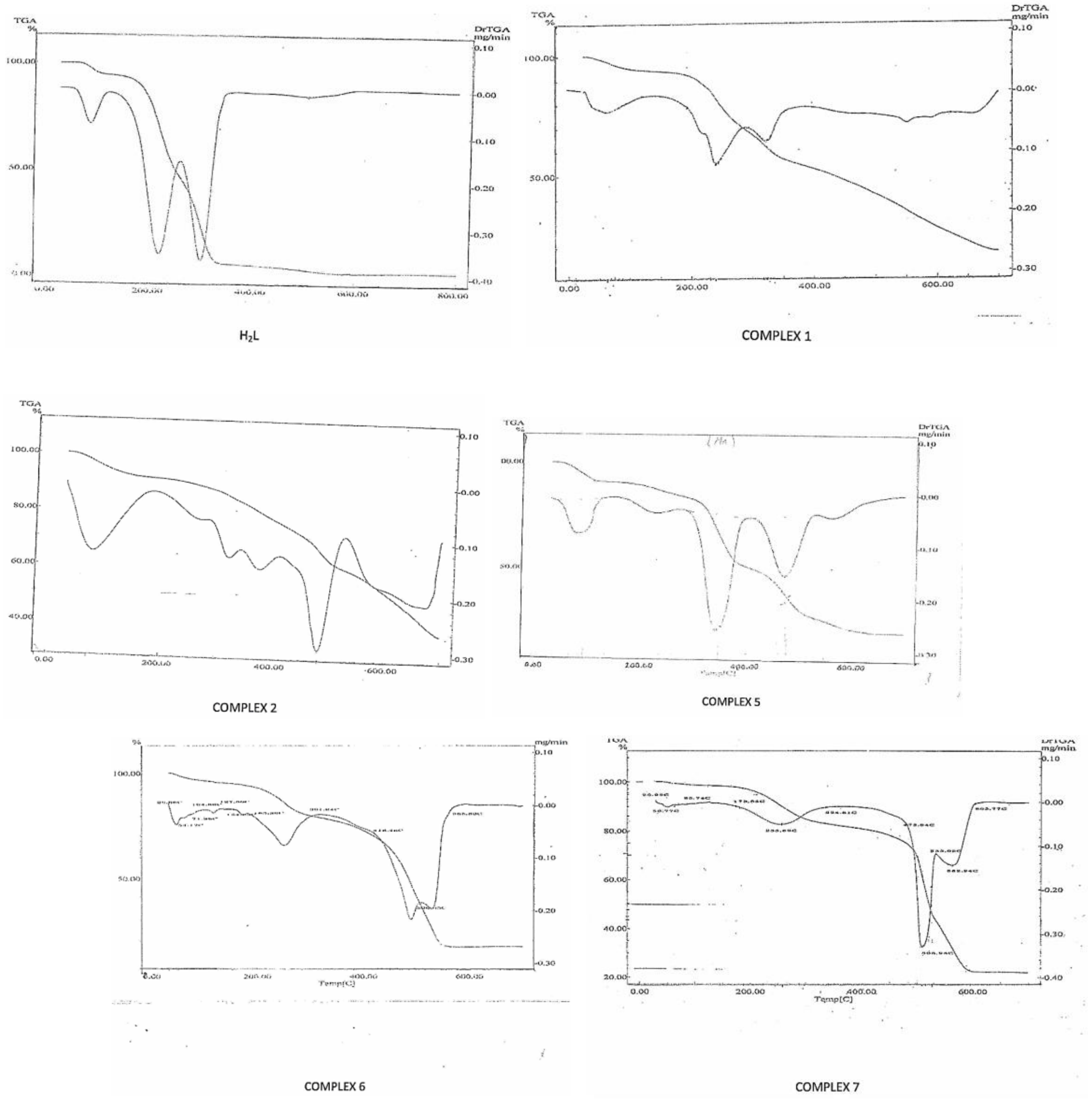

H_2L COMPLEX 1

COMPLEX 2 COMPLEX 5

COMPLEX 6 COMPLEX 7

Figure 3. TGA and DTG curves of investigated complexes

Complex 7 is stable at room temperature, upon heating (30-130°C) a calculated weight loss due to removal of the all hydrated water molecules was (8.07% calcd. 7.94% found). The anhydrous complex was then decomposes pointed to pyrolysis and removal of one molecule of Cl_2 with mass loss (10.62% calcd.10.35% found) at the temperature range 130-474°C. While the third step of decomposition starts at 474°C and continuous up to 533°C corresponding to partial ligand pyrolysis with drastic weight loss (31.04% calcd. 31.10% found) which are in good agreement with the decomposition of ($C_{12}H_8N_4$).

The final step of decomposition occurs within the temperature range 533-600°C associated with broad endothermic peaks, which complete degradation of organic ligand (25.82% calcd. 25.8% found) corresponding to ($C_{10}H_{11}N_3$). Above 600°C the ultimate decomposition product (two mole of ZnO) is formed as a final product (found and calculated) weight loss is 24.29%, 24.3% respectively. Based on the above arguments, the proposed chemical structures for the prepared ligand and their complexes are shown in Figure 4.

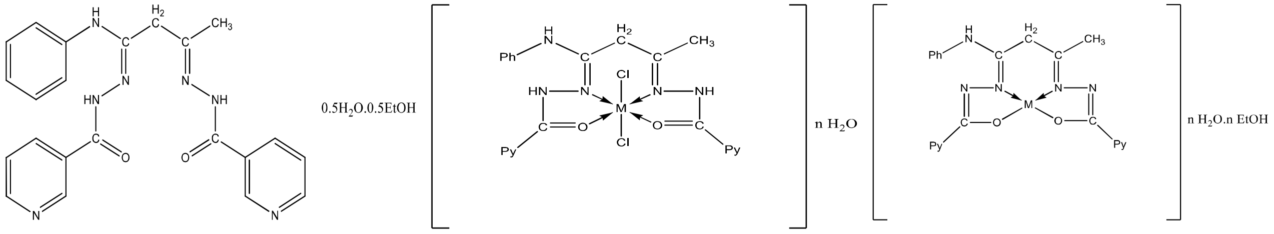

(H_2L)

Complex M n
1 Cu 3.5
2 Ni 5.5

Complex M n
3 Co 2.5
4 Zn 3.5

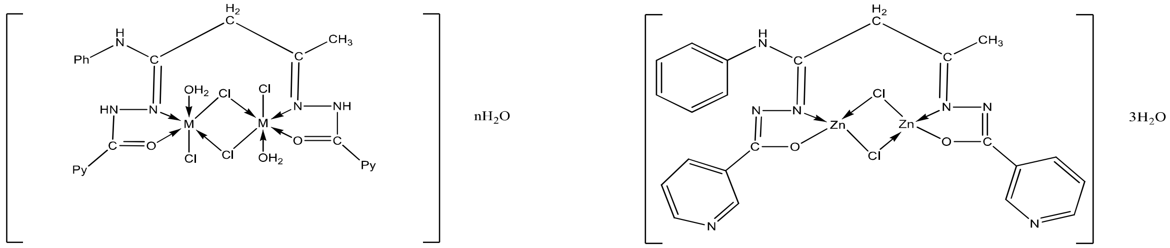

Complex M n
5 Mn 1
6 Co 0

Figure 4. Chemical structures for the prepared ligand and their complexes

Molecular Modeling

In view of hexa coordination, the present Cu and Ni complexes, M(L)Cl_2]nH_2O, (complexes 1,2) the molecular modeling of the compounds as representation based on their octahedral structures. In most cases, the actual bond angles and lengths are close to the optimal values, and the proposed structures are acceptable Figure 4.

In compounds 1,2 the Cu-O and Ni-O are 1.8179, 1.8177 A° and the two long M-Cl bond being trans to each other. When the M-O (Cu or Ni) bonds are included, the four coordination geometry around the copper is close to square planar and ι equal to 0. As a result the Cu or Ni atoms exists in octahedral geometry in which the basal plane is defined by four N_2O_2 and axial position is occupied by two Cl (β=trans angle/2=89.9~90) as shown in Figure 5.

The structure analysis of cobalt complex reveals that, the two diagonal angles of coordination sphere are 120°C-

112˚C (O$_4$—Co—Cl$_7$, N$_1$—Co—Cl$_6$) and the four angular projections by the four bonds are 96-60. Hence, a well-established planar geometry, the coordination geometry is ascertained by the observed ι value for four coordinated complexes ι$_4$=360-(α+β)/141 ι$_4$ will range from 1 for perfect tetrahedral to zero for a perfect square planner geometry and (0.85-0.82) for trigonal pyramid. The four coordinations around cobalt is (O$_4$—C$_{l6}$—C$_{l7}$—N$_1$) close to ι=0.87 and the geometry of Co in basal plane may be distorted tetrahedral [38,39] (Figure 5).

Table 4. Thermal analyses (TG/DTG) data of the ligand (H$_2$L) and its metal complexes

N	Compound	TG range (°C)	DTG Peak (°C)	Mass Loss%		Assignment	T$_s$ (°C)
				Calcd.	Found		
	H$_2$L	49-172	84 (m)	7.16	7.14	Loss of 0.5 mol of EtOH and 0.5 mol of H$_2$O$^{(b)}$	172
		172-265	220 (s)	47.43	47.46	Partial ligand pyrolysis$^{(d)}$ (C$_{12}$H$_8$N$_2$O$_2$)	
		265-562	301 (s)	42.28	42.42	Complete ligand pyrolysis$^{(d)}$ (C$_9$H$_{11}$N$_5$)	
1	[Cu(L)Cl$_2$]3.5H$_2$O	27-217	63 (br)	10.29	10.2	Loss of 3.5 mol of H$_2$O	
		125-285	239 (m)	11.59	11.55	Loss of Cl2	254
		285-360 360-573	321 (w) 550 (vw)	36.9	36.87	Partial ligand pyrolysis (C$_{12}$H$_{10}$N$_4$O$_2$)	
		573-756	643 (br)	28.24	28.25	Complete ligand pyrolysis (C$_{10}$H$_{11}$N$_3$`)	
		At 756°C		12.99	13	(CuO)	
2	[Ni(L)Cl$_2$] 4H$_2$O	30-290	79 (m)	15.37	15.4	Loss of 4 mol of H$_2$O	
		290-412	322 (w) 377 (w)	11	10.78	Loss of Cl$_2$	377
		412-526	482 (s|)	18.78	18.48	Partial ligand pyrolysis (C6H5N2O)	
		526-800	674 (br)	43.2	43.12	Complete ligand pyrolysis (C$_{16}$H$_{16}$N$_5$)	
		At 900°C		11.59	11.55	(NiO)	
3	[Co(H$_2$L)] 2.5H$_2$O.0.5ETOH	31-133	103 (S)	4.3	4.37	Loss of 0.5 mol of EtOH	
		133-225	235 (S)	8.33	8.25	Loss of 2.5 mol of H$_2$O	225
		225-426	319 (W)	45.38	48.3	Partial ligand pyrolysis	
		426-695	458 (W) 563 (br)	30.49	30.52	Complete ligand pyrolysis	
		At 695		10.9	11.16	(CoO)	
4	[Zn(H2L)]3.5H2O	31-217	92 (w)	11.63	11.64	Loss of 3.5 mol of H2O	217
		217-407	236 (s)	46.2	46.18	Partial ligand pyrolysis	
		407-897	344 (W)	27	27.1	Complete ligand pyrolysis	
		At 897				(ZnO)	
5	[Mn$_2$(L)Cl$_4$.2H$_2$O] H$_2$O	33-118	84(m)	7.4	7.4	Loss of 3 mol of H2O	
		118-381	353(s)	19.7	19.72	Loss of Cl4	353
		381-524	484(m)	28.86	28.88	Partial ligand pyrolysis (C12H8N4)	

		524-676	574 (br)	24	24.05	Complete ligand pyrolysis ($C_{10}H_{11}N_3$)	
		At 676 C		19.42	19.45	(2MnO)	
6	[Co_2(L)Cl_4.$2H_2O$]	31-130	108 (br)	5.06	5.07	Loss of 2 mol of H_2O	
		130-387	250 (m)	19.98	20	Loss of Cl_4	387
		387-528	489 (m)	29.26	29.1	Partial ligand pyrolysis (C12H8N4)	
		528-567	530 (w)	24.34	24.36	Complete ligand pyrolysis ($C_{10}H_{11}N_3$)	
		At 567°C		21.08	21.05	(2CoO)	
7	[Zn_2(H_2L)Cl_2]$3H_2O$	29-130	51 (w)	8.06	7.94	Loss of 3 mol of H_2O	
		130-474	400 (br)	10.6	10.35	Loss of Cl_2	400
		474-533	509 (s)	31.04	31.1	Partial ligand pyrolysis (C12H8N4)	
		533-600	562 (m)	25.82	25.8	Complete ligand pyrolysis ($C_{10}H_{11}N_3$) forming 2ZnO	

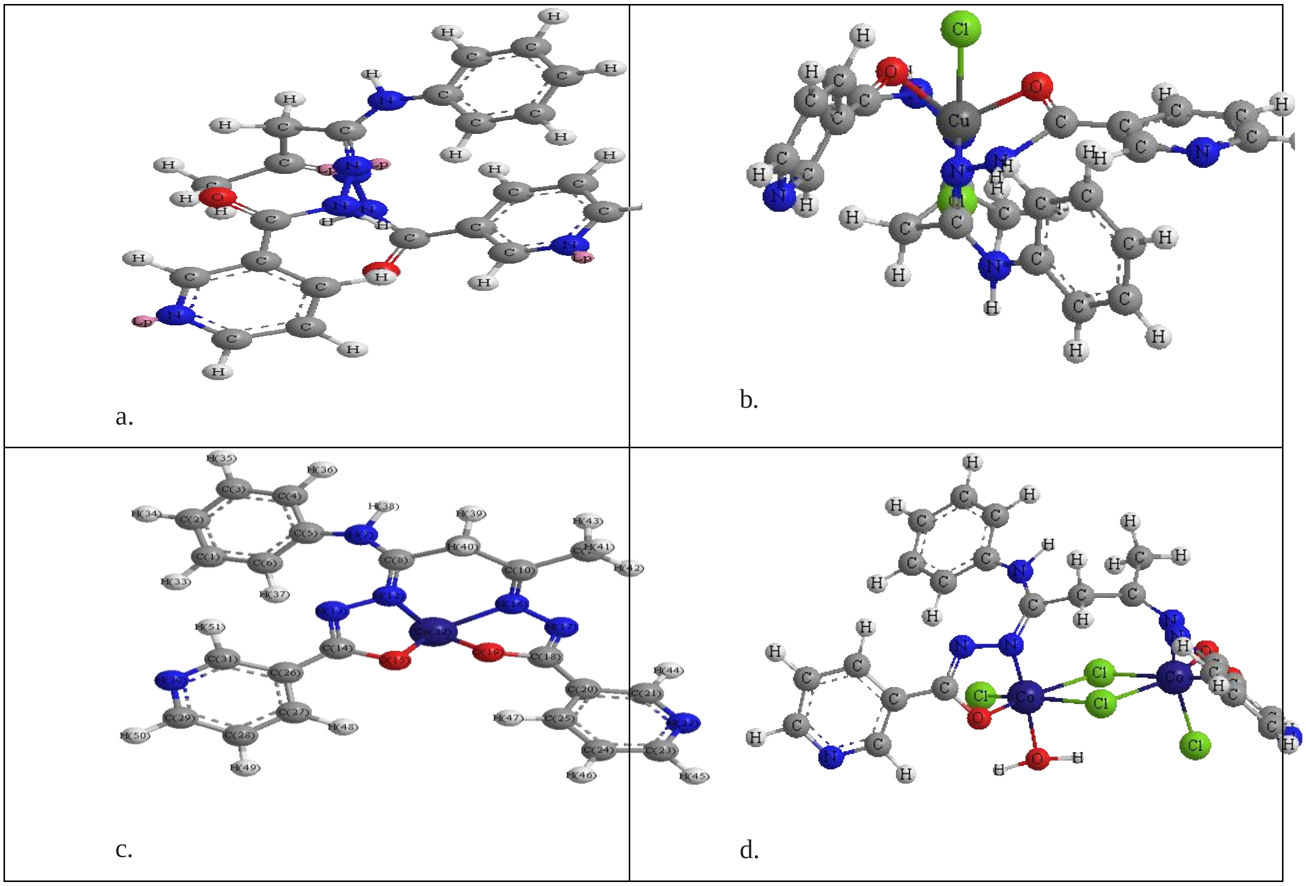
a. b. c. d.

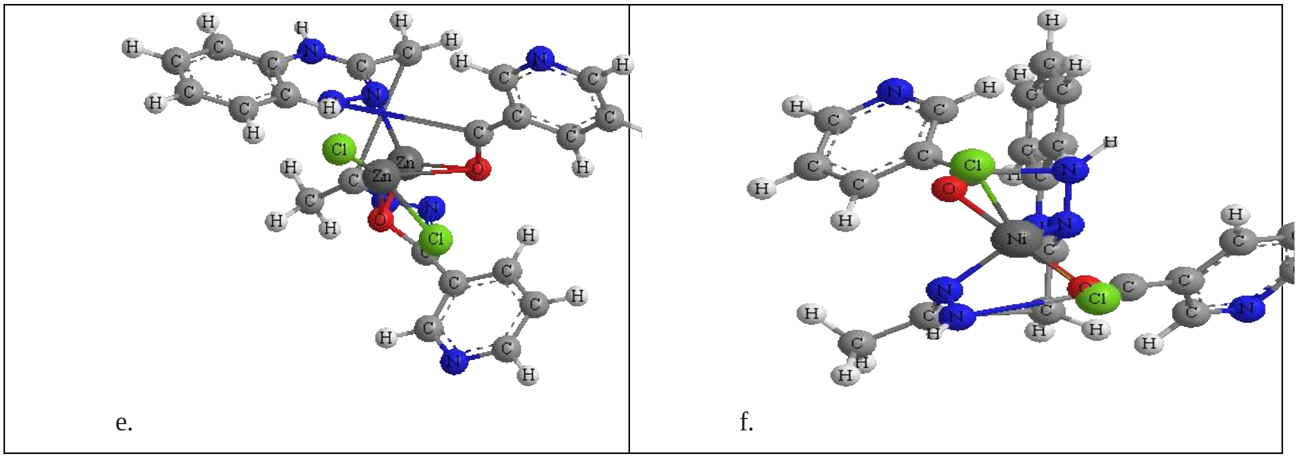

e. f.

Figures 5a-5e. Molecular modeling

In the Zn (II) coordination environment, the distance (Zn—Cl, Zn—Cl=1.899A$^{\circ}$) and (Zn—N, Zn—O=1.930A$^{\circ}$) are very similar to those found in other tetrahedral Zn (II) complex with the $NOCl_2$ coordination mode [17-39]. The major distortion from ideal tetrahedral geometry is found in the (O—Zn—N) angle of 87.4°, (Cl—Zn—N_1)=113.8. However it is noteworthy that Cl—Zn—O angle of 112.96 is the next major distortion from ideal geometry.

The deviation from perfect tetrahedral is evident from ideally linear trans angle Cl—Zn—N=113.89 which shows slight deviation from 120°. The coordination polyhedron around each Zn (II) is the best described as tetrahedral and is ascertained by the observed τ values. The values of τ_4 will range from=1 for perfect tetrahedral geometry to zero for perfect square planar and 0.85 for perfect trigonal pyramidal [40-42]. From the obtained data indicate that τ value equal to 0.95 from $ZnNOCl_2$ chromophor and 0.15 from indicating distorted squar planar and finally τ =0.96 for the hypothical chromo phore is suggesting distorted tetrahedral. As shown in Figure 5.

X- Ray

Table 5 represents the XRD spectral data for the ligand and its copper complex including the values of the Bragg angle (28) the ß at (FWHM), the inter planar spacing (d) and the calculated particle size (D) in nm. The particle size of the complex at (28) 21.84 was estimated using the well-known Debye-Scherer formula given in Eq.

$D=K\lambda/ß \cos\theta$ was found to be 28.96 nm and its disclose to 0.00244 n and for ligand

D=20.68 nm and its disclose=0.0017 nm for ligand smaller than Cu complex.

These values confirmed that the particle size are located within the narrow scale range except Co complexes which show one of them is amorphous and the other is poly crystalline as shown in the following Figure 6.

Transmission Electron Microscopy (TEM)

TEM analysis revealed the morphology of the samples and allowed deduction of mean particle size, it sometimes show the shape of nano particles. The particles of ligand and its metal complexes in the Nano scale size and shapes of particles have been examined by the TEM photographs as shown in Figure 7. The TEM of ligand exhibits aggregation and collective particles as shown as a dark view with irregular structure. Whereas, the ligand containing transition metal ions (Cu, Ni, Co), the crystallinity have been increased which indicated by the increased crystal size as well as the formation of the ring pattern in the nano size.

The average sizes are predicted from Figure 7 were nearly from (3.6-8.43) nm respectively. It is concluded that the Cu and Ni complexes micro structure are similar in scale size and smaller than the Co complex due to the difference in chemical composition of the complexes.

Table 5. The XRD spectral data

Compound	**Maximum peak (2θ)**	**D**	**1/D^2**	**FWHM**
Ligand	18.46	20.68	0.00234	0.4066
The average		27.065	0.001714	
Cu complex	21.84	28.96	0.0012	0.2919
The average		85.658	0.0024	

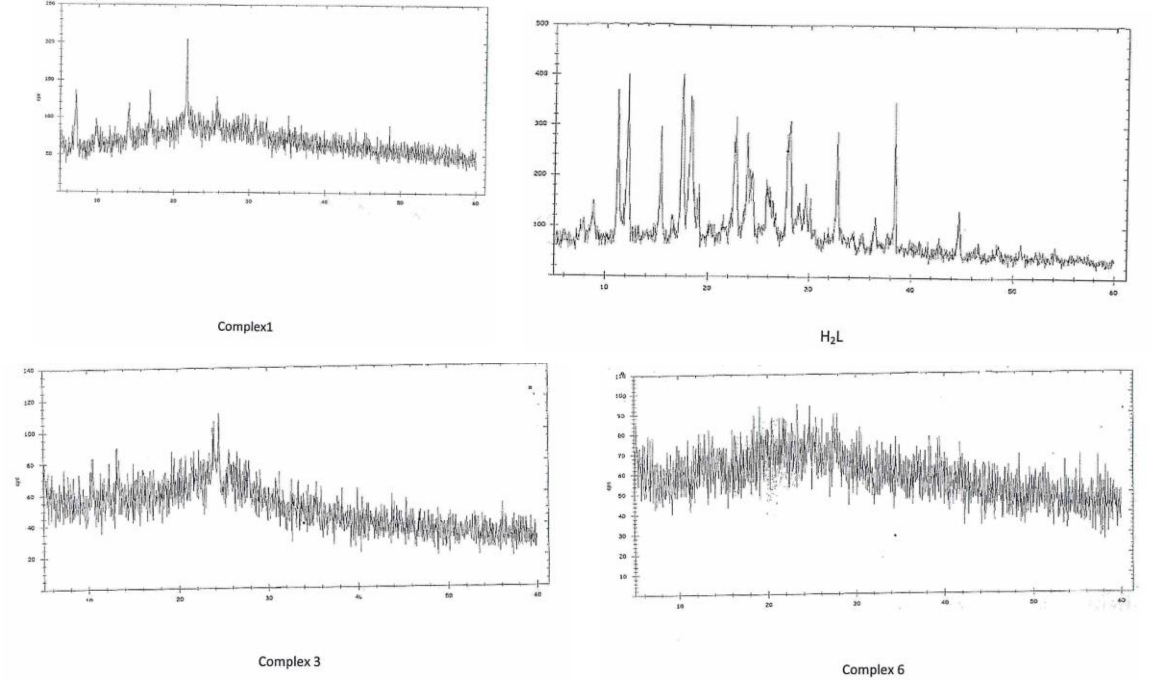
Complex1

H_2L

Complex 3

Complex 6

Figure 6. X-ray

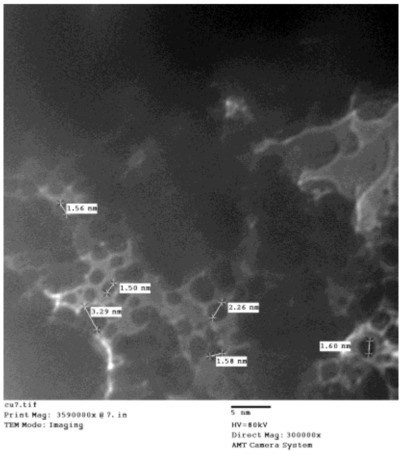

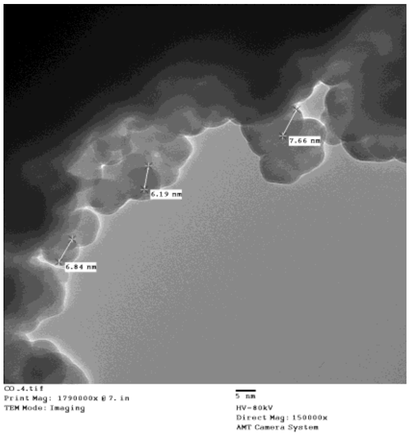

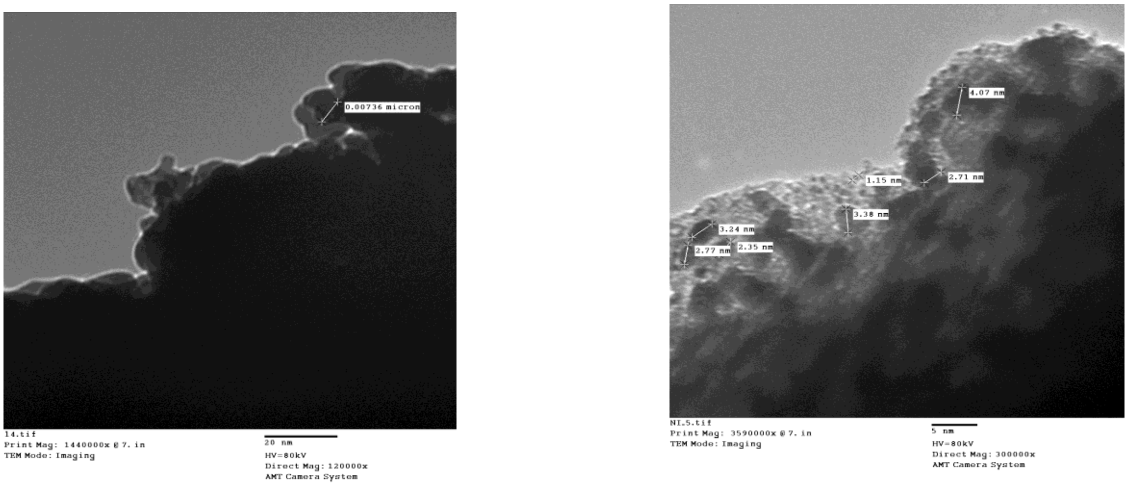

Figure 7. The average crystal sizes

Catalytic Studies of the Ligand and Its Complexes on MB

When Methylene Blue dye (MB) was added to hydrogen peroxide in the absence of the complexes 1,5,6,7 as catalyst no changes in the absorption spectrum have been observed indicating that H_2O_2 alone is unable to degrade the MB dye. The reaction was initiated when each complex was added as catalyst. The final solution is completely bleached as illustrated by the absorption spectra of MB in water at (λ_{max} = 667 nm) at the beginning and end of the reaction Figure 4 show the absorbance of MB in water before and after the reaction with H_2O_2 in presence of the complexes as catalyst. It is showed that in absence of complexes, it was observed a negligible change in absorbance at 667 nm, indicating the catalytic activity of the new complexes, the catalytic activity was found to follow the order Cu(II)>Mn(II)>Co(II)>Zn(II) Table 6, the difference in catalytic activities of different complexes may be explained on the basis of change in nature of metal.

Methylene blue dye (MB), used in wide range in textile industry, has been found to be toxic, stable in waste water stream, difficult to decompose and causes water pollution [43] So that, it is important to depredated this dye in to simple molecules to overcome the environment pollution. The photo catalytic activities of the complexes were evaluated by degradation of MB in water as illustrated in literatures [44]. As shown in Figure 8, the absorption spectra were recorded. Clearly, the gradual decrease in the concentration of MB dye and the photo degradation efficiency %D was calculated use the equation:

$$\%D=(C_0-C_t/C_0) \times 100 \sim (A_0 - A_t/A_0) \times 100$$

Where C_0 is the intial concentration of dye solution and C_t is its concentration at time (t). These can be substituted by the initial absorbance A_0 and the absorbance at time (t) At respectively and the rate of the reaction can be calculated according to pseudo first order reaction according to the following equation:

$$\text{Ln } A_0/A_t=K_{obs}\, t$$

Where A_0 and A_t are the absorbance of MB dye at time 0 and t , K_{obs} ~ pseudo first order rate constant. The observed maximum degradation efficiency of MB is about 96%.

Table 6. Metal complexes degradation

The catalyst complexes	The percentage of degradation	The time
Cu(d^1)	96%	At 60 min.
Mn(d^5)	65%	
Co(d^7)	61%	
Zn(d^{10})	49%	

Anticancer Studies

The Anticancer activity of the ligand (1) and some of its metal complexes were evaluated against HEPG-2 cell line and shown in Figures 9 and 10. In this study, we try to know the chemotherapeutic activity of the tested complexes by comparing them with the standard drug (IMURAN (azathioprine)) (Figure 11). The treatment of the different complexes in DMSO showed similar effect in the tumoral cell line used as it was previously reported. The solvent DMSO shows no effect in cell growth. The ligand shows a weak inhibition effect at ranges of concentrations used, however, the complexes showed a better effect against HEPG-2 cell lines.

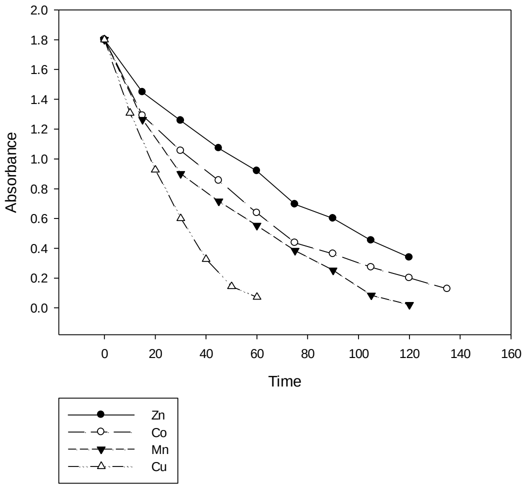

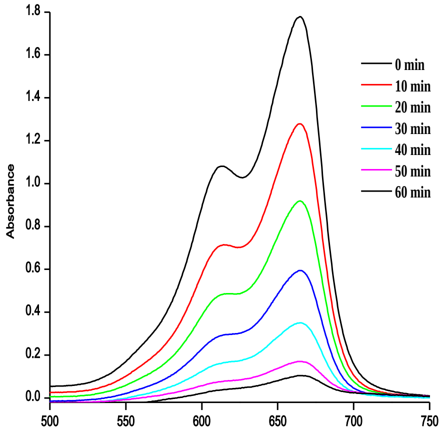

complex 1

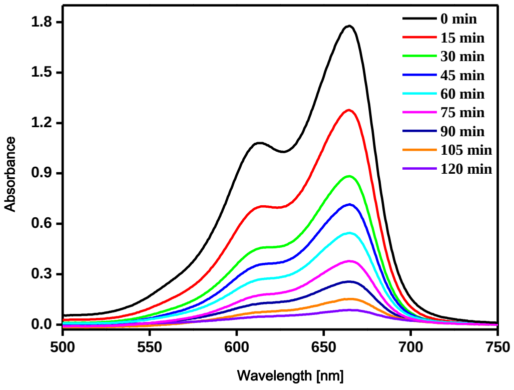

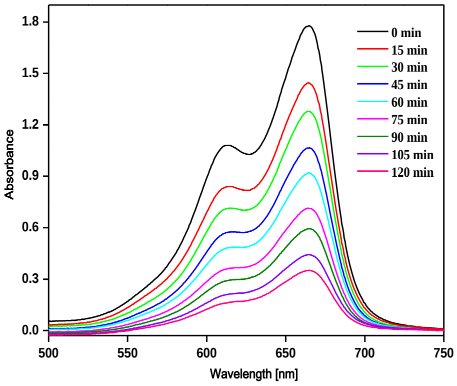

Complex 5

complex 7

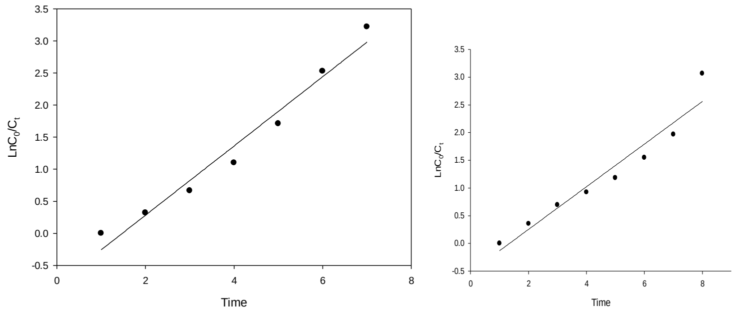

(Cu) R=0.9843, K_{os}=0.0433 (Mn) R=0.9657, K_{os}=0.0423

Figure 8. The absorption spectra

The obtained data indicate the surviving fraction ratio against HEPG-2 tumor increasing with the decrease of the concentration in the range of the tested concentrations. Cytotoxicity results indicated that the tested Cu(II) complex, Ni(II) complex and Zn(II) (IC_{50} 50.2, 15.5 and 29.7 µg ml^{-1}, respectively) demonstrated potent cytotoxicity against HEPG-2 cancer cells while Mn (II) complex demonstrated the most potent cytotoxicity against HepG2 cancer cells with IC50=479 (Figure 4). The chemotherapeutic activity of the complexes may be attributed to the central metal atom which was explained by Tweedy's chelation theory. Also, the positive charge of the metal increases the acidity of coordinated ligand that bears protons, leading to stronger hydrogen bonds which enhance the biological activity. Moreover, Gaetke and Chow had reported that metal has been suggested to facilitate oxidated tissue injury through a free-radical mediated pathway analogous to the Fenton reaction. By applying the ESR-trapping technique, evidence for metal-mediated hydroxyl radical formation in vivo has been obtained. Reactive oxygen species are produced through a Fenton-type reaction as follows:

$LM(II)+H_2O_2 \rightarrow LM(I)+.OOH+H+$

$LM(I)+H_2O_2 \rightarrow LM(II)+.OH+OH-$

Where L, organic ligand.

Furthermore, metal could act as a double-edged sword by inducing DNA damage and also by inhibiting their repair. The OH radicals react with DNA sugars and radicals react with DNA sugars and bases, resulting in the release of free bases and strand break occurs. Bases and the most significant and well characterized of the OH reactions is hydrogen atom abstraction from the C4 on the deoxyribose unit to yield sugar radicals with subsequent β-elimination. By this mechanism strand break occurs as well as the release of the free bases. Another form of attack on the DNA bases is by solvated electrons, probably *via* a similar reaction to those discussed below for the direct effects of radiation on DNA [45,46].

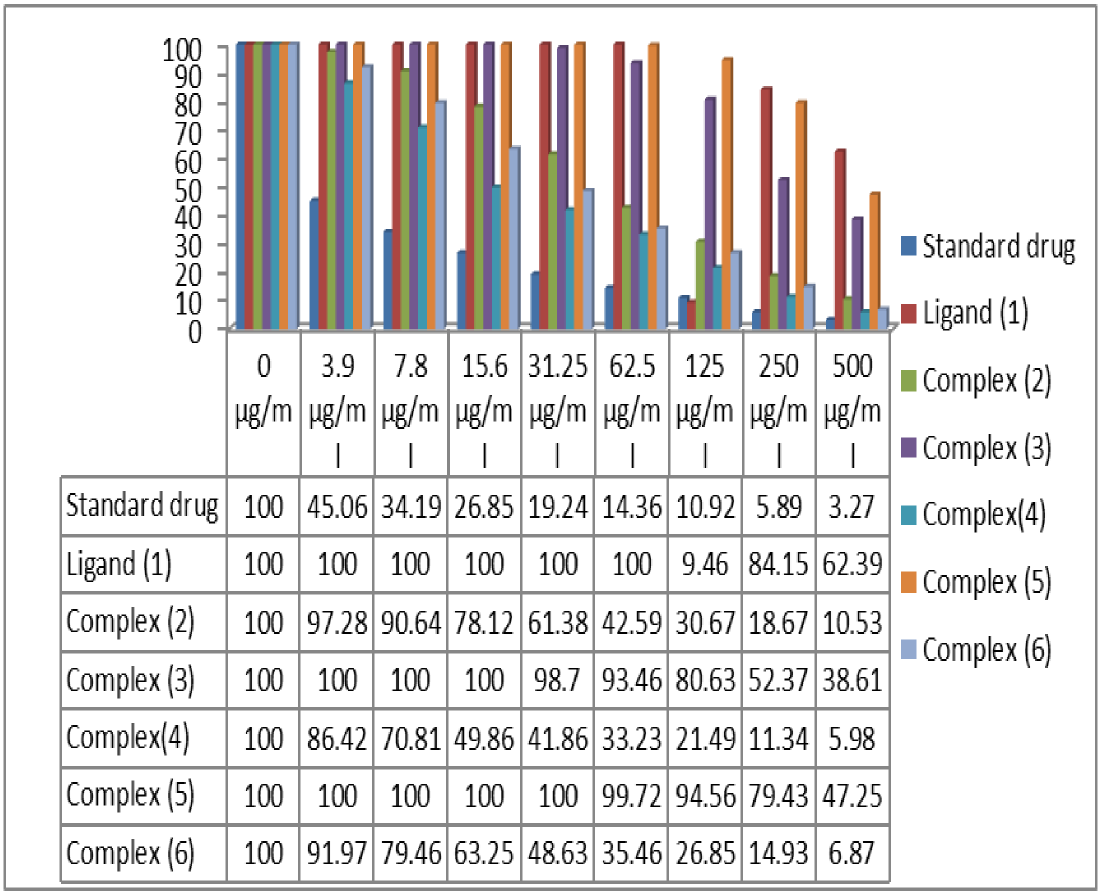

	0 µg/ml	3.9 µg/ml	7.8 µg/ml	15.6 µg/ml	31.25 µg/ml	62.5 µg/ml	125 µg/ml	250 µg/ml	500 µg/ml
Standard drug	100	45.06	34.19	26.85	19.24	14.36	10.92	5.89	3.27
Ligand (1)	100	100	100	100	100	100	9.46	84.15	62.39
Complex (2)	100	97.28	90.64	78.12	61.38	42.59	30.67	18.67	10.53
Complex (3)	100	100	100	100	98.7	93.46	80.63	52.37	38.61
Complex(4)	100	86.42	70.81	49.86	41.86	33.23	21.49	11.34	5.98
Complex (5)	100	100	100	100	100	99.72	94.56	79.43	47.25
Complex (6)	100	91.97	79.46	63.25	48.63	35.46	26.85	14.93	6.87

Figure 9. Evaluation of Anticancer activity of ligand, H_2L (1) and its metal complexes against human hepatic HEPG-2 Cell Line

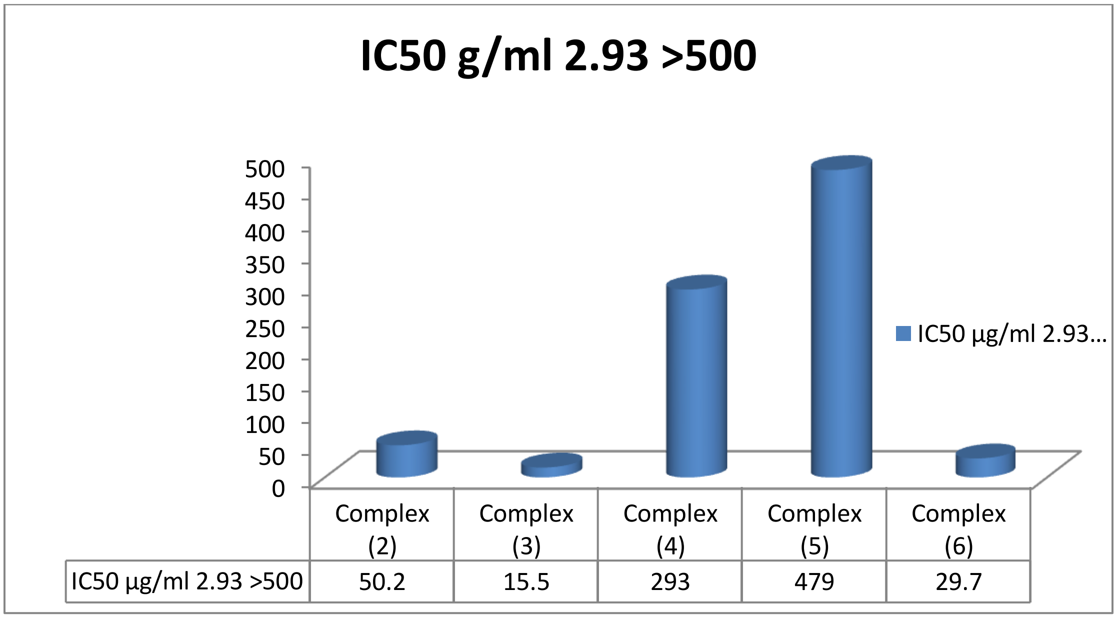

	Complex (2)	Complex (3)	Complex (4)	Complex (5)	Complex (6)
IC50 µg/ml 2.93 >500	50.2	15.5	293	479	29.7

Figure 10. IC_{50} values of ligand and some of its complexes (2),(3), (4), (5) and (6) against human hepatic HEPG-2 cell lines

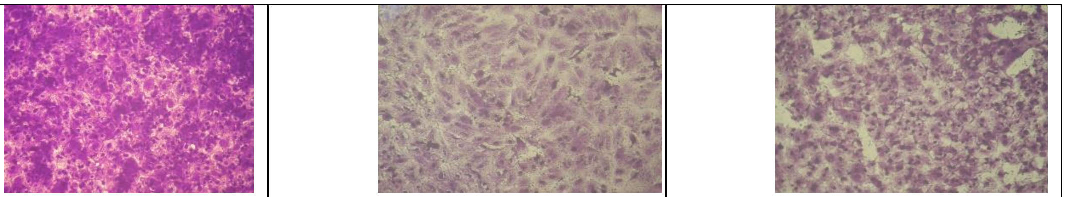

Standard Ligand Complex(3)

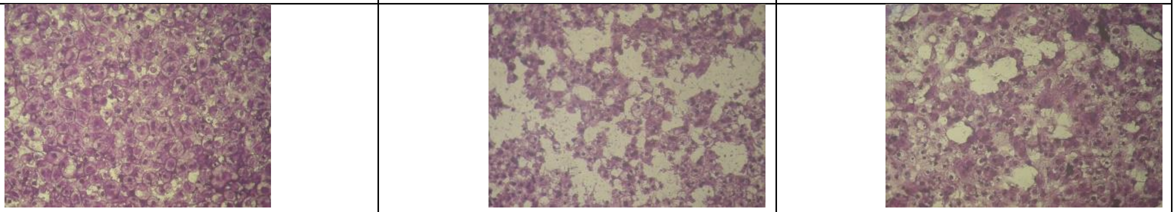

Complex (**4**) Complex (**6**) Complex (**7**)

Figure 11. Chemotherapeutic activity of the tested complexes by comparing them with the standard drug (IMURAN (azathioprine))

CONCLUSION

Synthesis, Characterization using different spectroscopic methods, thermal behavior was studied as well as TEM and XRD, In addition Catalytic and Cytotoxic Activities were studied.

REFERENCES

1. H Adams; DE Fenton; G Minardi; E Mura; M Angelo. *Inorg Chem Commun*. **2000**, 3: 24-28.
2. ZY Yang; RD Yang; FS Li; KB Yu. *Polyhedron*. **2000**, 19: 2599-2604.
3. M Kuriakose; MRP Kurup; E Suresh. *Polyhedron*. **2007**, 26: 2713-2718.
4. R Gup; B Kirkan. *Spectrochim Acta*. **2005**, 62: 1188-1195.
5. SQ bao; LU Zhong Lin; Wu Xiao Li; May Xiang. *Trans Met Chem*. **1994**, 19, 503-505.
6. ZL Lu; CY Duan; YP Tian; XZ You; HK Fun; K Sivakumar. *Acta Crystal*. **1996**, 52: 1507-1509.
7. S Fucharion; RT Rowley; NW Paul Eds Thalassemia. *Pathophysiology and Management*. **1988**, Part B, Alan R. Liss, New York.
8. R Montes; JJ Laserna; *Anal Sci*. **1991**, 7: 467-471.
9. RB Singh; P Jain; RP Singh. *Talanta*. **1982**, 29: 77.
10. S El-din H Etaiw; Dina; H Marie. *Inorg and organo met poly and mat*. **2018**, 28, 508-518.
11. MI Ayad. *Arabian Journal of Chemistry*. **2016**, 9: S1297-S1306.
12. Maiti; Amalendu; Ghosh; Sakiprosad. *Indian J Chem*. **1989**, 28: 980-983.
13. CNR Rao. *Academic press, New York*. **1963**, 260-262.
14. MS Masoud; SA AbouEl-Enein; IM Abed; AE Ali. *J Coord Chem*. **2002**, 55(2): 153.
15. ZH Abd El-Wahab; MM Mashaly; AA Salman; BA El-shetary; AA Faheim. *Spectrochim Acta part*. **2004**, 60: 2861.
16. DK Rastogi; D Sahnisk. *J Inorg Nucl Chem*. **1980**, 42: 323.
17. MM Mostafa; KM Ibrahim; MNH Moussa. *Trans Met Chem*. **1984**, 9: 243.
18. DK Rastogi; D Sahnisk; VB Rana; S Duak Dua. *J Inorg Nucl Chem*. **1979**, 41: 21.
19. J Albert; A Caonzalezb; J Granell; R Moragas; X Solans; M Fontbardia. *Chem Soc Dallen Trans*. **1998**,

1781.

20. R Gap; M Kirkan. Spectro Chem Acta.**2005**, A 62,1188.
21. S Naskar; D Mishra; RJ Butcher;SK Chattopadhyay. Polyhedron.**2007**, 26, 3703.
22. MFR Fouda; MM Abd El Zaher; MME Shakdofa; FA El Saied; MI Ayad; AS El-Tabel. *Trans Met Chem*. **2008,** 33: 219-228.
23. H Koksal; M Dolaz; M Tumer; S Serin. *Synth React Inorg Met Org Chem*. **2001**, 31(7): 1141-1162.
24. OA El-Ceammal; EA Elmorsy; YE Shereif. *Spectro Chim Acta A Mol Biomol Spectroscopy*. **2014**, 120: 332.
25. SA Sallam; AS Orabi; BA ElShetary; A Lentz. *Trans Met Chem*. **2002**, 27: 447.
26. AS El-Table; SA El-Enein. *Coord Chem*. **2004**, 57: 281.
27. KG Ragunathan; PK Bharaduaj. *Chem Soc Dalton Trans*. **1992**, 2417.
28. PK Panda; SB Mishra; BK Mohapatka. *Inorg Nucl Chem*. **1980**, 42, 497-499.
29. D Kuwar; PK Gupta; A Syanal. *Chem Soc Sci*. **2005**, 117: 247.
30. SM Emam; SA AbouEL-Enein; FA Elsaied; SY Elshater. *Spectro chem Acta*. **2012**, 92-96.
31. HM El-Table; FA Saied; MI Ayad. *Inorg Met Org chem*. **2002**, 32(7): 1189.
32. MI Ayad; AS El-Tabl. *Pol J Chem*. **1990**, 73: 263.
33. G Sperier; J Csihony; AM Whalen; CG Pierpont. *T Inorg Chem*. **1996**, 35: 3519-3524.
34. D Kivelson; R Neiman. *J Chem Phys*. **1961**, 35: 149-155.
35. BJ Hathaway; DE Billing. *Coord Chem*. **1970**, 5: 143-207.
36. R Olar; M Badea; E Cristurean; C Parnau; D Marinescu. *Therin Anal Cal*. **2006**, 84: 53.
37. HA El-Boraey; AM Donia; MF El-Samalehy. *Anal Pyrol*. **2005**, 73: 204.
38. AW Addison; TN Rao; J Reedijk; JV Rijn; GC Verschoor. *Chem Soc Dalton Trans*. **1984**, 1349-1356.
39. EL Muetterties; LJ Guggenberger. *Am Chem Soc*. **1974**, 96: 1748.
40. JA Lewis; BL Iran; DT Puerta; EM Rumberger; DN Hendrickson; SM Cohen. *J Chem Soc Dalton Trans*. **2005**, 2588.
41. S Gupta; A Mukherjee; M Nethaji; AR Chakravarty. *Polyhedron*. **2005**, 24: 1922.
42. AW Addison; TN Rao; J Van Rijn; GC Verschoor. *J Chem Soc Dalton Trans*. **1984**, 1349.
43. S EL-Din; H Etaiw; TA Fayed; MM El-bendary; H Marie. *J Inorg Organomet Polym*. **2017**, 27: 1391.
44. S EL-Din; H Etaiw; H Marie. *Solid State Sciences*. **2018**, 77: 5-13.
45. T Mosmann. *J Immunol Methods*. **1983**, 65: 55-63.
46. SM Gomha; SM Riyadh; EA Mahmmoud; MM Elaasser. *Heterocycles*. **2015**, 91(6): 1227-1243.